Journal of Network Intelligence
Taiwan Ubiquitous Information
 ISSN 2414-8105 (Online)
Volume **10**, Number **3**, August **2025**

Analysis of UWB-based Automotive Keyless Entry System Localization

Weidong Fang, Zheng Zhang*, Zibiao Chen

School of Electronic, Electrical Engineering and Physics
Fujian Provincial Key Laboratory of Automotive Electronics and Electric Drive
Fujian University of Technology, Fuzhou 350118, China
wdfang@126.com, onlyzhangzheng@163.com, 13348229520@126.com

Jeng-Shyang Pan

College of Computer Science and Engineering
Shandong University of Science and Technology, Qingdao 266590, China

Chaoyang University of Technology, Taichung 413310, Taiwan
jengshyangpan@gmail.com

Kai He

Decoration Department of Fuyao Group
Fuyao Glass Industry Group Co., Ltd, Fuzhou 350301, China

Central South University, Changsha 410083, China
kai.he01@fuyaogroup.com

*Corresponding author: Zheng Zhang

Received January 17, 2024, revised October 8, 2024, accepted March 17, 2025.

Abstract. *Ultra Wide Band (UWB) technology is rapidly advancing and emerging as a new trend in key localization for automotive keyless entry systems. Due to factors such as multipath effects and Non-Line-of-Sight (NLOS) conditions, significant errors in distance estimation can occur. To address the NLOS issue caused by vehicle body obstruction, a simulated automotive unlocking localization system was constructed using a four-base station-to-one-tag positioning system based on the Weighted Least Squares (WLS) + UWB algorithm. The four base stations simulated the size of the vehicle and polled the tag for distance information. The distance information was filtered using the Unscented Kalman Filter (UKF), and the WLS positioning algorithm was applied to calculate the coordinates of the tag, enabling the assessment of unlocking errors and positioning errors between the car key and the vehicle's location. The experimental findings provide evidence for the efficacy of WLS+UWB in mitigating the occurrence of vehicle misunlocking and enhancing the precision of car key localization in NLOS environments.*
Keywords: Ultra-wideband, Time of flight ranging, Unscented kalman filter, Weighted least squares, Localization system

1. **Introduction.** With the increasing demand for people to rely on vehicles for travel, car keyless entry (KES) has become a new trend to solve vehicle access solutions [1]. The driver only needs to carry the vehicle key, and the vehicle can determine the estimated position of the key label. When the key approaches the vehicle, the vehicle can automatically unlock. When the tag key is a certain distance away from the car, the car can be properly locked [2]. Nowadays, most PKE systems use low-power Bluetooth and digital NFC key technology to complete the key positioning. Bluetooth's distance range is based

on signal strength, with short communication distance, poor accuracy, easy interference in a communication frequency band, and insufficient security [3]. NFC key has an extremely short communication distance and poor penetration, which makes it difficult to unlock in a non-line-of-sight environment.

However, as a new wireless communication technology, UWB technology has the characteristics of high precision, low energy consumption, and insensitive to channel fading [4], so UWB technology has been widely used in various positioning fields [5]. In the case of line of sight (LOS), centimeter-level positioning can be achieved [6]. However, when facing the non-line of sight(NLOS) environment, the UWB communication signal between the base station and the tag will be completely blocked by obstacles, resulting in large fluctuations in the discontinuous error of key tag positioning [7], thereby reducing the accurate position between the vehicle body and the vehicle key.

Figure 1 shows the NLOS status of the vehicle keyless entry system due to the body occlusion. The four base stations are respectively arranged on both sides of the front of the car and both sides of the parking space. The time of flight (TOF) is used to measure the distance from the tag to the base station [8]. The label is on the LOS path, i.e. $d0$ and $d1$ paths, to measure more accurate distance information. When the tag is on the NLOS path, that is, $d2$ and $d3$ paths, the error is large. Table 1 shows the actual distance and TOF measurement distance as well as the relative error. As shown in Table 1, the relative error between the true distance and the measured distance is shown. The relative error in the NLOS environment is large, even more than 40%. Therefore, the distance in the NLOS environment may lead to a large error in label positioning, and the vehicle unlocking failure.

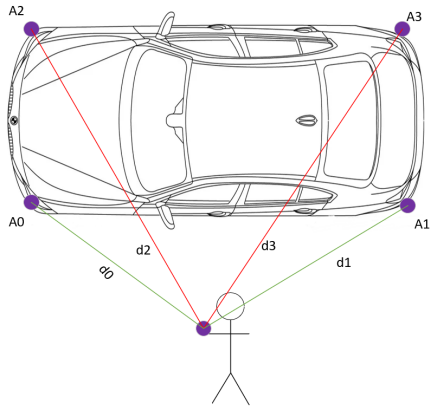

Figure 1. Keyless entry system NLOS test diagram

Table 1. LOS and NLOS comparison errors

Path	Real distance (m)	Measuring distance (m)	Relative error
d0	1.69	1.91	13.01%
d1	1.70	1.88	10.58%
d2	2.68	3.83	42.91%
d2	2.69	3.92	45.72%

2. **Related work.** To address the problem of degradation of UWB positioning accuracy in NLOS wireless transmission environments, researchers are exploring and developing various solutions. Zheng et al. proposed a fusion method of Neural Network and Linear Coordinate Solver (NN-LCS) using two FC layers to extract the distance feature and the received signal strength (RSS) feature and using a multilayer perceptron (MLP) to estimate the distance of these two feature fusions [9]. Thang et al. used the Support Vector Machine Classification (SVR) technique to identify NLOS signals to improve the accuracy and proposed a new localization algorithm Two-Step Iterative Algorithm (TSI), which improves the localization accuracy and extends the range of the localization, but it is difficult to be deployed due to its high complexity [10]. Yao et al.'s use of a time-of-arrival-based ranging method (TOA) does not take into account clock drift between devices and will result in increased errors [11]. Zhong et al. solved the time synchronization problem by connecting all UWB modules to the master via optical fiber, but it increased the complexity and cost of system deployment [12]. Zhang et al. developed the Distance-KF method and the Position-KF method by extending the conventional Kalman filtering approach to address the challenges posed by NLOS environments. These methods aim to enhance the accuracy of positioning. However, when applied to handheld tags, they may result in increased ranging errors. [13]. Feng et al. built an indoor positioning system using a combination of Extended Kalman Filter and Traceless Kalman Filter under different line-of-sight environments with a priori information provided by the Inertial Measurement Unit (IMU), which improved the robustness and accuracy, but the complexity of the algorithms increased the complexity of the deployment of the base station [14]. Wang et al. used a particle filtering algorithm to fuse the data from two UWB and two IMU sensors, and improved the sampling accuracy of each step by adding a priori information from IMU, so that fewer particles can be used to approximate the true a posteriori probability distributions, and improved the accuracy of fused positioning [15]. Li et al. used UWB positioning to improve the performance of PDR by reducing the cumulative distribution error in PDR, calibrating the tilt effect of smartphones, improving heading estimation, and using Kalman filtering as a fusion algorithm, the fused indoor positioning algorithm outperformed the single positioning algorithm [16]. Liu et al. used UWB for tunnel construction workers using the symmetry-based bilateral bidirectional ranging method, wavelet threshold denoising of positioning results for moving targets to reduce the effect of outliers on UWB positioning and improve positioning accuracy [17]. Li et al. used EKF to fuse UWB and IMU data to obtain attitude, velocity, and position. Subsequently, the velocity and output measurements are combined with the odometer output using complementary filtering techniques to enhance the overall accuracy. [18].

3. System algorithm design.

3.1. UWB ranging algorithm.

At this stage, there are four commonly used ranging methods for UWB, which are based on Time of Arrival (TOA) [19], Time Difference of Arrival (TDOA), Angle of Arrival (AOA)/Phase Difference of Arrival (PDOA), and Received Signal Strength Indicator (RSSI). In this paper, Double-Sided Two-way Ranging (DS-TWR) based on time of arrival is selected, which is further classified into Asymmetric Double-Sided Two-way Ranging (SDS-TWR) and Symmetric Double-Sided Two-Way Ranging (SDS-TWR) based on whether the response time is symmetric or not [20], ADS-TWR in the ranging process of time control is more flexible and does not require time synchronization between the base station and the label, effectively reducing the crystal offset [21], so this paper adopts ADS-TWR ranging method.

The schematic diagram of a single ADS-TWR method for one ranging is shown in Figure 2. Device A sends a signal with a time stamp to device B at the T1. Device B receives the signal with a ranging request at T2 and after time Treply1, sends a ranging request signal to device A at T3, device A receives the signal at T4, and after time Treply2, makes a second ranging request to device B at T5. Device B receives the second ranging request at the T6 moment to complete the single bilateral bidirectional ranging.

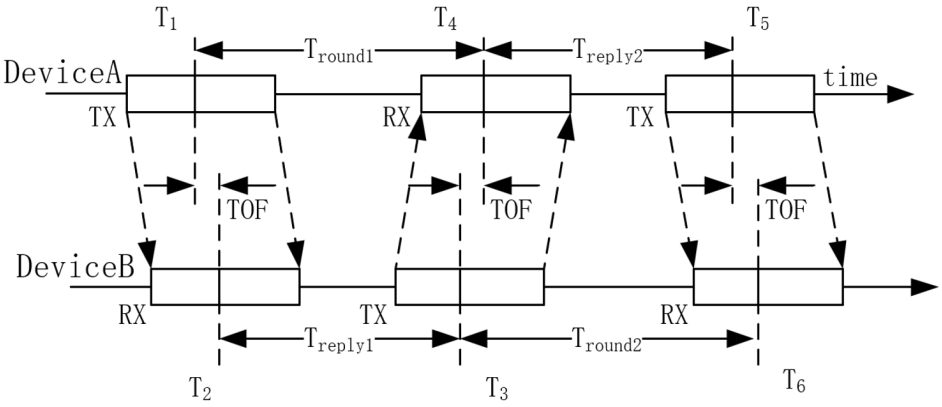

FIGURE 2. ADS-TWR schematic diagram

In the ADS-TWR process, the data frames sent by each device carry timestamp information, and Tround1 represents the time used by device A from transmitting the signal to receiving the signal, and Tround2 represents the time used by device B from transmitting the signal to receiving the signal. For ADS-TWR response time is not symmetric, i.e., Treply1 and Treply2 are not required to be kept equal, and the time of flight and distance between the two devices can be calculated by calculating the TOF of the UWB signal between devices A and B through Equation(1):

$$TOF = \frac{(T_{round1} \times T_{round2}) - (T_{reply1} \times T_{reply2})}{T_{round1} + T_{reply1} + T_{round2} + T_{reply2}} \tag{1}$$

Since there is a clock frequency deviation between the devices, it is assumed that the crystal frequency offset of devices A and B are e_A , e_B. The unit is ppm, and the $\hat{TOF}$ can be estimated as shown in Equation (2):

$$\hat{TOF} = \frac{T_{round1}(1+e_A) \times T_{round2}(1+e_B) - T_{reply1}(1+e_B) \times T_{reply2}(1+e_A)}{T_{round1}(1+e_A) + T_{reply1}(1+e_B) + T_{round2}(1+e_B) + T_{reply2}(1+e_A)} \tag{2}$$

Simplification gives the flight time between the two devices A,B as shown in Equation (3):

$$TOF = \frac{(1+e_A)+(1+e_B)}{2(1+e_A)(1+e_B)} \hat{TOF} \tag{3}$$

The final distance between the two devices is shown in Equation (4):

$$S = TOF \times c \tag{4}$$

where S is the distance between device A and device B, and c is the speed of light, $c = 3 \times 10^8$m/s.

3.2. **Weighted least squares mathematical model.** The weighted least squares method does not require a priori information about the positioning system and can more accurately predict the estimated value distance information in the LOS case [22] to obtain the least sum of squares of the Euclidean distance error, which is modeled based on the ADS-TWR ranging algorithm, As shown in Equation (5):

$$Y = AX + b \tag{5}$$

where Y is a known $k \times 1$ dimensional vector representing the value from the measured distance value to the observed value, X is an unknown $n \times 1$ dimensional vector representing the position of the locator tag, A is a $k \times n$ dimensional matrix of measurement coefficients representing the relationship between the measured value and the locator tag, and b is a $k \times 1$ dimensional vector that satisfies the expectation $E(b) = 0$ and has a covariance $cov(b) = \sigma^2 G$, where G is a known positive definite matrix and σ^2 is the unbiased estimate. Then the residuals can be expressed as in Equation (6):

$$r = AX + b - Y \tag{6}$$

The weighted least squares based method to locate the tag position X is shown in Equation (7):

$$Q(X) = (Y - b - AX)^T W (Y - b - AX) \tag{7}$$

where W is the weighting matrix of the measurements at each base station, the first-order derivation of Equation (7) is performed, and the result is made equal to 0, as shown in Equation (8):

$$\frac{\partial Q_W(X)}{\partial X} = -2A^T WY + 2AWXY = 0 \tag{8}$$

Then Equation (8) is useful as a unique Equation solution as shown in Equation (9):

$$\hat{X} = (A^T WA)^{-1} A'WY \tag{9}$$

The coordinates of the position of the positioning tag in three-dimensional space can be calculated.

3.3. **Improvement of localisation accuracy by unscented kalman filter.** Unscented Kalman filter (UKF) is the addition of Unscented transform (UT) to the traditional Kalman filter to deal with the nonlinear transfer problem of mean and covariance in nonlinear systems [23], where a series of deterministic samples are used to approximate the a posteriori probability densities and does not require approximation of a nonlinear function and does not need to be derived from the Jacobi matrix [24]. The state space model of UKF for a nonlinear system is shown in Equation (10):

$$\begin{cases} X(k) = F(x(k), W(k)) \\ Z(k) = H(x(k), M(k)) \end{cases} \tag{10}$$

where k is the time variable; X_k and Z_k are the system state vector and observation vector at moment k. $F(\cdot)$ is the system state transfer function. $H(\cdot)$ is the observation function. R_k is the system process noise. W_k is the observation noise.

Step1: Assuming that the mean and covariance of the state vector X_k are $\bar{x}$ and p_k, the $2n + 1$ Sigma sampling points and their weights are obtained according to the UT transform as show in Equation (11):

$$\begin{cases} X_k^{(0)} = \bar{x} \\ X_k^{(i)} = \bar{x} + (\sqrt{(n+\theta)p_k})_i, i = 1, 2, \ldots, n \\ X_k^{(i)} = \bar{x} - (\sqrt{(n+\theta)p_k})_{i-n}, i = n+1, n+2, \ldots, 2n \end{cases} \tag{11}$$

As shown in Equation (12), $\theta = \alpha^2(n+k)$ is the scaling parameter. α is the discrete parameter, describing the degree of dispersion of the set of Sigma points from $\bar{x}$, usually taken as 0.01. k is the subsampling factor, usually set to θ; β is the state distribution parameter of the system, and for the Gaussian distribution, $\beta = 2$ to take the optimal. ω_m and ω_c are the weights of the mean and the covariance. $\sqrt{(n+\theta)p_k}$ is the square root of the covariance matrix p_k; $\left(\sqrt{(n+\theta)p_k}\right)_i$ is the i-th column of the matrix ordinary root $\sqrt{(n+\theta)p_k}$.

$$\begin{cases} \omega_m^{(0)} = \dfrac{\theta}{n+\theta} \\ \omega_c^{(0)} = \dfrac{\theta}{n+\theta} + 1 - \alpha^2 + \beta \\ \omega_m^{(i)} = \omega_c^{(i)} = \dfrac{\theta}{2(n+\theta)}, i = 1, 2, \cdots, 2m \end{cases} \tag{12}$$

Step2: The calculated Sigma point set is used as an input to the system state transfer function $F(\cdot)$ to obtain the predicted transformed result $X_{k|k-1}^{(i)}$, and the mean $\overline{X}_k$ and covariance $\overline{P}_k$ are calculated based on the predicted system state quantities as shown in Equation (13):

$$\begin{cases} X_{k|k-1}^{(i)} = F(X_{k-1|k-1}^{(i)}), i = 1, 2, \cdots, 2m \\ \overline{X}_k = \sum_{i=0}^{2m} \omega_m^{(i)} X_{k|k-1}^{(i)} \\ P_{\overline{X}_k} = \sum_{i=0}^{2m} \omega_c^{(i)} (X_{k|k-1}^{(i)} - \overline{X}_k)(X_{k|k-1}^{(i)} - \overline{X}_k)^T + Q_k \end{cases} \tag{13}$$

As show in Equation (13) the mean $\overline{X}_k$ is the predicted value of the state vector X_k, $P_{\overline{X}_k}$ is the covariance of $\overline{X}_k$, and Q_k is the covariance matrix of the systematic error W_k.

Step3: Substitute the predicted mean $\overline{X}_k$ and predicted covariance $P_{\overline{X}_k}$ into Equation (11), and get the new Sigma point set after UT transformation, and substitute the new Sigma point set into the observation function $H(\cdot)$ to get the observation vector $Z_{k|k-1}^{(i)}$ of the new Sigma point set, and the covariance $P_{\overline{Z}_k}$ of the mean $\overline{Z}_k$ and $\overline{Z}_k$ are computed from $Z_{k|k-1}^{(i)}$ as shown in Equation (14):

$$\begin{cases} Z_{k|k-1}^{(i)} = h(X_{k-1|k-1}^{(i)}), i = 1, 2, \cdots, 2m \\ \overline{Z}_k = \sum_{i=0}^{2m} \omega_m^{(i)} Z_{k|k-1}^{(i)} \\ P_{\overline{Z}_k} = \sum_{i=0}^{2m} \omega_c^{(i)} (Z_{k|k-1}^{(i)} - \overline{Z}_k)(Z_{k|k-1}^{(i)} - \overline{Z}_k)^T + R_k \end{cases} \tag{14}$$

As shown in Equation (14) mean $\overline{Z}_k$ is the observed value of the observation vector Z_k, $P_{\overline{Z}_k}$ is the covariance of $\overline{Z}_k$, and R_k is the covariance matrix of the observation error V_k. The correlation covariance between the predicted and observed values of the system is calculated from Equation (13) and Equation (14) as shown in Equation (15):

$$P_{\overline{X}_k \overline{Z}_k} = \sum_{i=0}^{2m} \omega_c^{(i)} (X_{k|k-1}^{(i)} - \overline{X}_k)(Z_{k|k-1}^{(i)} - \overline{Z}_k)^T \tag{15}$$

Step4: Calculate the traceless Kalman filter gain K_k, correct the predicted value X_k, and update the state equation as shown in Equation (16):

$$K_k = P_{\overline{X}_k \overline{Z}_k} P_{\overline{Z}_k - 1} \tag{16}$$

The state update equation, covariance update equation is shown in Equation (17):

$$\begin{cases} X_k = \overline{X}_k + K_k(Z_k - \overline{Z}_k) \\ P_k = P_{\overline{X}_k} + K_k P_{\overline{Z}_k} K_k^T \end{cases} \tag{17}$$

As shown in Equation (17), X_k is the state vector optimum, P_k is the covariance of the optimum X_k, $(Z_k - \overline{Z}_k)$ is the observation residual, and $K_k(Z_k - \overline{Z}_k)$ is the weighting of the observation residuals by using the untraceable Kalman filter gain.

Step5: Based on the state vector optimal result X_k and the optimal result covariance P_k, calculate the Sigma point set at moment k to find the optimal result of the state vector at moment $k+1$.

4. **Related experimental setup.**

4.1. **System overview.** To carry out the system evaluation, this paper builds a vehicle positioning system based on four base stations and one tag, with a single tag acting as a remote key. The workflow of this system is shown in Figure 3.

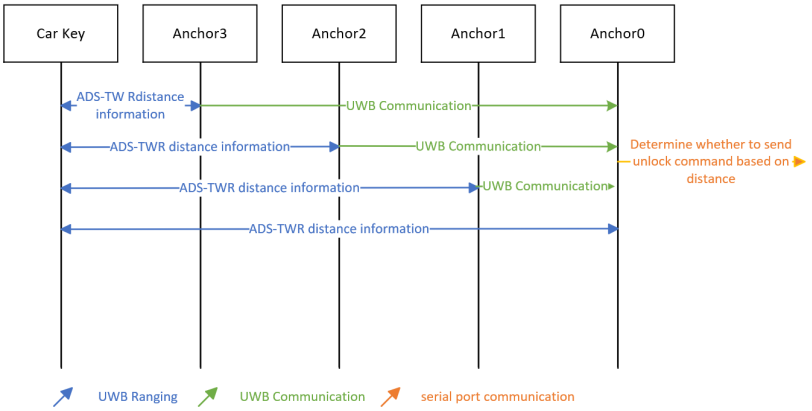

FIGURE 3. System workflow diagram

In this system, the control module and collection module are implemented based on STM32F103RCT6, and the peripheral circuits include reset circuits, LED indicator modules, power supply modules, and so on. The main base station is connected to the main base station through the Dupont cable to receive and process the data measured by the four base stations to the tag. the UWB base station/tag adopts the DW1000 chip designed by Decawave, with a data rate of 110 Kbps, channel 2, and an operating frequency of 3.5GHz∼4.2GHz, and adopts the FPC antenna to make the signals more stable and note that hardware can change the mode of base stations and tags through AT commands. The final ranking results are uploaded to the PC through the $A0$ base station, and the hardware connection diagram is shown in Figure 4:

4.2. **Experimental tests.** The traditional three-sided positioning algorithm cannot measure the label position on the diagonal outside the base station, so the weighted least squares positioning and optimized three-sided positioning algorithm are used for error comparison analysis. The experimental location is outdoors in the south area of Fujian

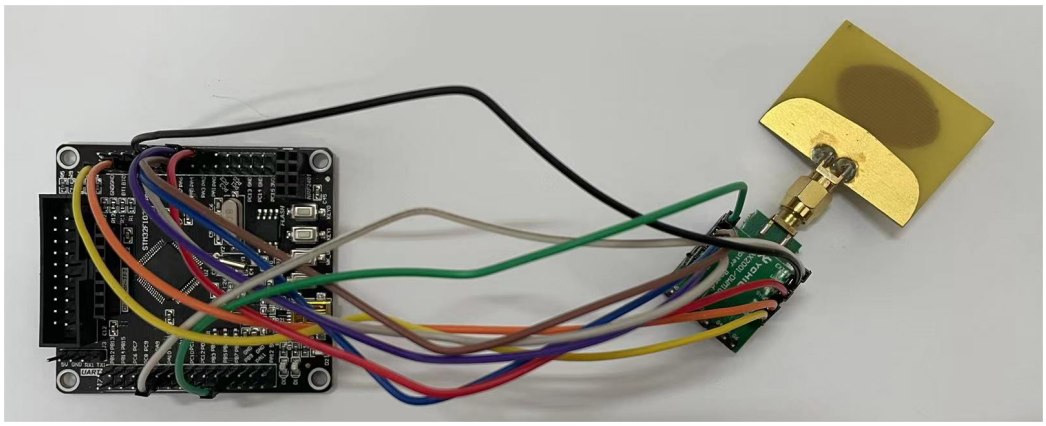

FIGURE 4. Hardware connection diagram

University of Technology, and the test point is sampled and tested, and the real system setup scenario is shown in Figure 5:

FIGURE 5. Experimental testing scenarios

In this paper, a four-base station approach is used for testing. Set the base station coordinates to $bs0$ (0,0), bs1 (4,0), bs2 (4,2), and bs3 (0,2) based on the length, width, and height of the car. Set the base station height to match the height of the car body to 108cm. Connect the base station bs0 to the PC to transmit the collected data and conduct the following two sets of experiments.

(1) Vehicle dynamic unlocking trajectory

Use the black trajectory 1 meter outside the vehicle body as the vehicle unlocks the trajectory, and unlock the vehicle when the key tag enters the interior of the 1-meter trajectory. The specific testing process is as follows: the handheld tag moves forward at a constant speed of $1m/s$ along a 1m trajectory, simulating the dynamic situation of the driver around the vehicle body. The dynamic trajectory is shown in Figure 6, and the coordinates of the four base stations represent the length and width of the vehicle body.

Figure 6 represents the behavioral trajectories in the NLOS environment without UKF for the optimized trilateral localization algorithm and the weighted least squares localization algorithm, respectively, and Figure 7 represents the trajectory routes after UKF. Comparing the two, it can be seen that the optimized trilateral localization has a large error in the diagonal region outside the base station, and the WLS algorithm fits the actual trajectory better. After UKF, both algorithms can fit the actual trajectory more gently. The optimized trilateral positioning algorithm still produces large errors in the

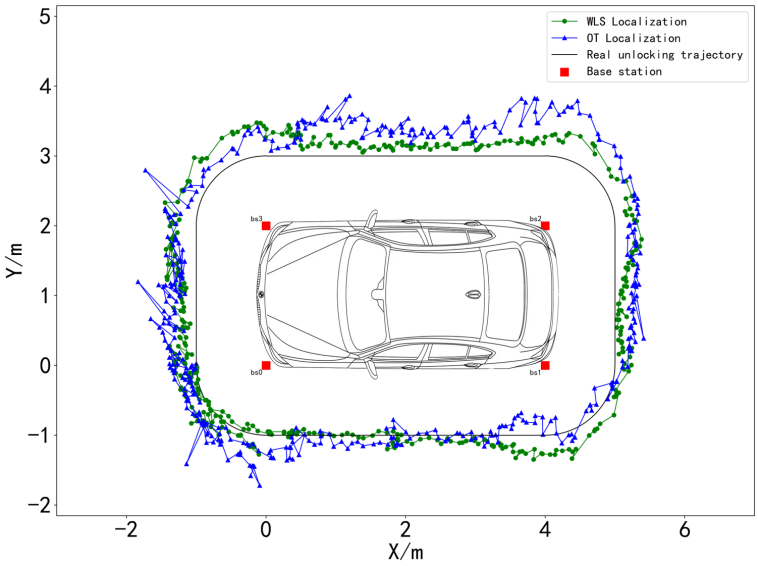

FIGURE 6. Unlocking trajectory of unfiltered vehicles

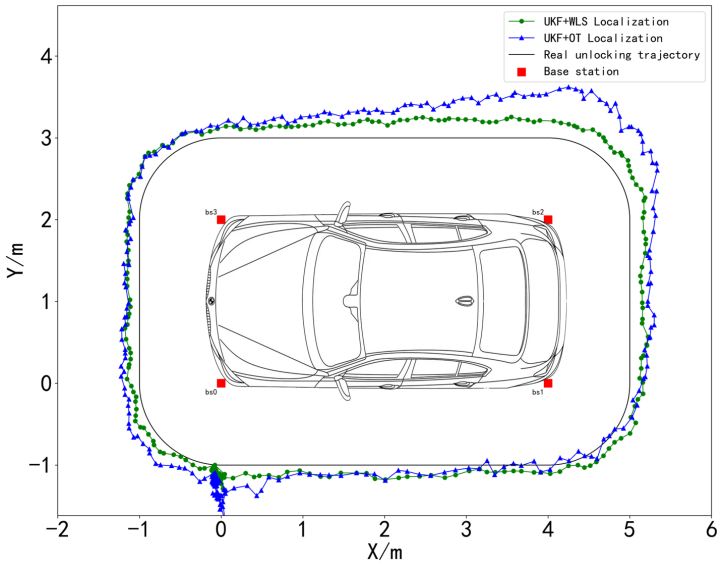

FIGURE 7. Unlocking trajectory of filtered vehicles

diagonal position. When the coordinates of the sampling points enter the unlocking range set by the vehicle, it is judged that the unlocking is successful. In the two experiments, the total number of sampling points without UKF filtering is 429, and the total number of sampling points after filtering is 321. Table 2 shows the number and proportion of unlocking failures for four different algorithms. The WLS positioning algorithm reduces the unlocking error by 1.4% compared to the trilateral positioning algorithm. The failure unlocking probability of UKF+WLS is 3.11% lower than that of the optimized trilateral positioning algorithm. After using the same positioning algorithm through UKF, the WLS accuracy improved by 8.23%, and the optimized trilateral positioning algorithm improved by 6.52%. The experiment shows that the UKF+WLS fusion algorithm can effectively reduce the probability of unlocking failure.

(2) Error test

TABLE 2. Algorithm error unlocking times and probability

Positioning algorithm	Unlocking failures (times)	Probability of unlocking failure (%)
Optimised trilateral	44	10.25
WLS	38	8.85
UKF+Optimised trilateral	12	3.73
UKF+WLS	2	0.62

Ten sets of static test points are preset on the vehicle unlocking trajectory, and each set of test points undergoes sixty distance tests. Error analysis is conducted before and after using two positioning algorithms and UKF filtering. The test results are shown in Figure 8 and Figure 9.

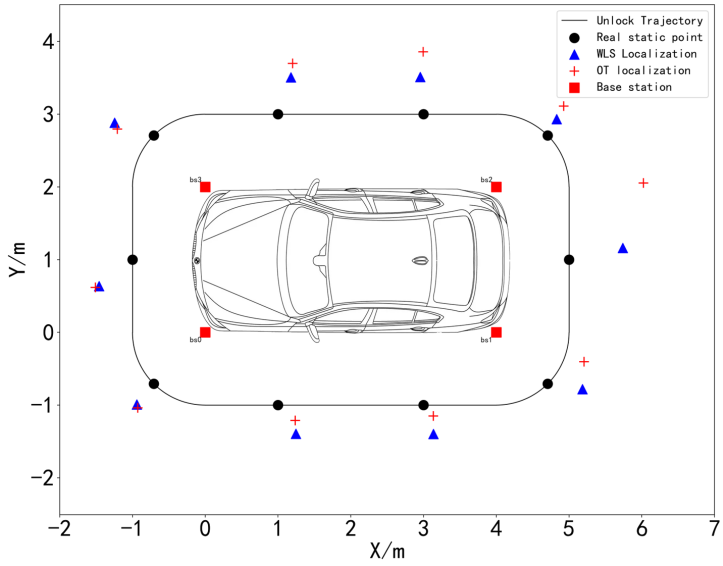

FIGURE 8. Static point measurement with unfiltering

As shown in Figure 8, before passing through UKF, WLS can be closer to real static points compared to the trilateral positioning algorithm, and the coordinate positioning accuracy is higher than that of the trilateral positioning algorithm. However, there are still some static sampling points with poor positioning accuracy, and the error fluctuation is still significant. As shown in Figure 9, both positioning algorithms, after being filtered by UKF, can effectively reduce error fluctuations. After reducing errors, they are closer to the true point coordinates and improve the probability of correct unlocking. It can be seen from Figure 10 that the error fluctuation range of the fusion algorithm after UKF+WLS is lower than the other three algorithms.

As shown in Table 3, the average error of both unfiltered positioning algorithms exceeds 0.5m, and the error fluctuates greatly. For the UKF-based trilateral positioning algorithm, the average error is 0.208m. Although the average error is low, the error fluctuates greatly. When using the UKF+WLS fusion algorithm, the positioning performance is the best, with an average error of 0.496m, a minimum error of 0.1m, and a maximum error of 0.28m. The minimum error of the UKF+WLS fusion algorithm is slightly higher than that of the UKF+trilateral positioning algorithm, which may be due to the weight ratio

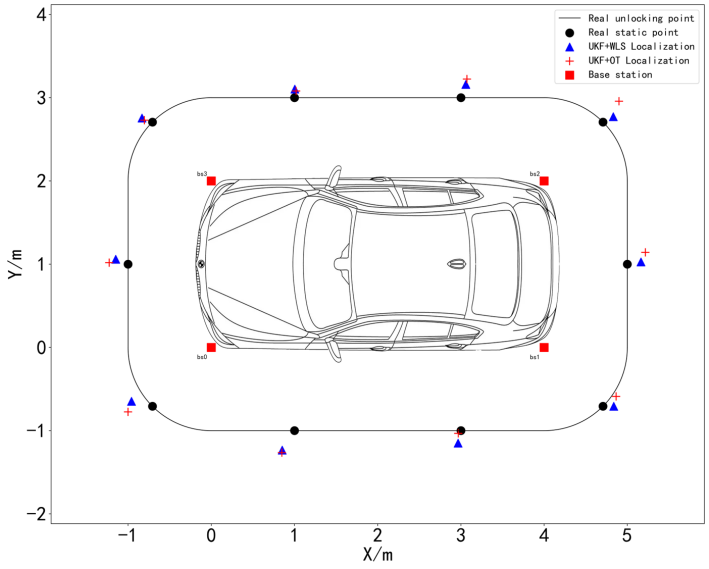

FIGURE 9. Static point measurement with filtering

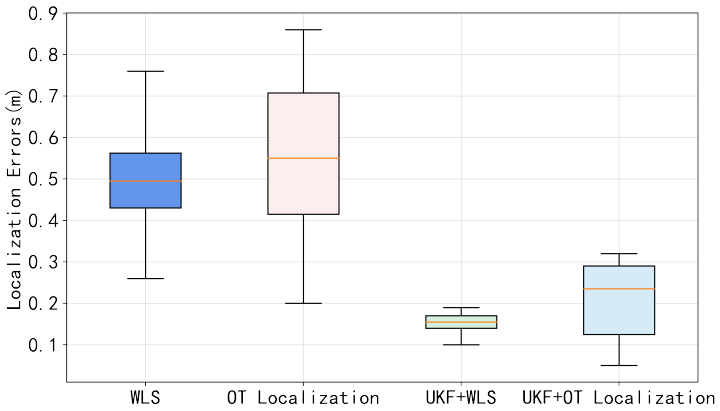

FIGURE 10. Boxplot of the localization error comparison

set by the four base stations in the weighted least squares method not fitting the actual situation of the vehicle.

TABLE 3. Algorithm error unlocking times and probability

Positioning algorithm	Minimum error (m)	Maximum error (m)	Average error (m)
Optimised trilateral	0.2	1.47	0.618
WLS	0.26	0.76	0.496
UKF+Optimised trilateral	0.05	0.32	0.208
UKF+WLS	0.1	0.28	0.17

5. **Conlusion.** This article focuses on the vehicle key positioning function in the keyless entry system of automobiles, using a new communication method to locate the key. By utilizing the characteristics of UWB signals to reduce the infection of various environmental signals, and using asymmetric bilateral bidirectional ranging method to obtain distance

data, the crystal oscillator error of the system can be effectively reduced. Then, through the process of unscented Kalman filtering, the distance information error caused by non-line-of-sight environmental issues is reduced. Finally, a weighted least squares positioning algorithm is proposed to obtain the precise position of the tag key. This study suggests the possibility of using UWB signals for communication in keyless entry systems. The results show that the comparison of experimental results through static sampling shows that the fusion algorithm with UKF has smaller positioning errors than the individual positioning algorithm, and the error fluctuation is significantly lower than that of the independent positioning algorithm. In addition, according to the sampling point data in the dynamic trajectory, it can be seen that the UKF+WLS fusion algorithm can reduce the error situation of erroneous unlocking. Based on the MCU equipped with the two algorithms, indicates that the system can quickly complete label localization even when deployed in inexpensive MCUs with low computing power. However, this article fixed the height of the tags and base stations, only considering the changes in tag positions in two-dimensional space, which will lead to different unlocking situations caused by changes in tag positions in three-dimensional space. In the future, we will introduce inertial measurement units to test the pedestrian gait movements of the human body as input to UKF, to more accurately predict the human movement status, and integrate IMU and UKF algorithms to achieve better system accuracy and robustness.

Acknowledgment. This research was funded by Fuzhou Science and Technology Plan Project: 2022-Q-009 and by Fujian University of Engineering and Fuyao Glass Industry Group Co., Ltd. Automotive Electronics and Electrical System Development Cooperation Project (GY-H-20108).

REFERENCES

[1] H. Sun, "Simulation method for automotive remote keyless application," SAE Technical Paper, Tech. Rep., 2021.

[2] M. Singh, M. Roeschlin, E. Zalzala, P. Leu, and S. Čapkun, "Security analysis of ieee 802.15. 4z/hrp uwb time-of-flight distance measurement," in *Proceedings of the 14th ACM Conference on Security and Privacy in Wireless and Mobile Networks*, 2021, pp. 227–237.

[3] M. Rogobete, M. I. Mihailescu, and E. Marin, "Ultra-wideband technology in telematics security-a short survey," in *2021 13th International Conference on Electronics, Computers and Artificial Intelligence (ECAI)*. IEEE, 2021, pp. 1–6.

[4] Y. Liu and Y. Bao, "Real-time remote measurement of distance using ultra-wideband (uwb) sensors," *Automation in Construction*, vol. 150, p. 104849, 2023.

[5] S. Li, G. Li, L. Wang, Y. Zhou, Y. Peng, and J. Fu, "A three-dimensional robust ridge estimation positioning method for uwb in a complex environment," *Advances in Space Research*, vol. 60, no. 12, pp. 2763–2775, 2017.

[6] C. Jiang, J. Shen, S. Chen, Y. Chen, D. Liu, and Y. Bo, "Uwb nlos/los classification using deep learning method," *IEEE Communications Letters*, vol. 24, no. 10, pp. 2226–2230, 2020.

[7] H. Zhang, Q. Wang, C. Yan, J. Xu, and B. Zhang, "Research on uwb indoor positioning algorithm under the influence of human occlusion and spatial nlos," *Remote Sensing*, vol. 14, no. 24, p. 6338, 2022.

[8] L. Schmid, D. Salido-Monzú, and A. Wieser, "Accuracy assessment and learned error mitigation of uwb tof ranging," in *2019 International Conference on Indoor Positioning and Indoor Navigation (IPIN)*, 2019, pp. 1–8.

[9] Z. Zheng, S. Yan, L. Sun, H. Shu, and X. Zhou, "Nn-lcs: Neural network and linear coordinate solver fusion method for uwb localization in car keyless entry system," *Sensors*, vol. 23, no. 5, p. 2694, 2023.

[10] T. Van Nguyen, Y. Jeong, H. Shin, and M. Z. Win, "Machine learning for wideband localization," *IEEE Journal on Selected Areas in Communications*, vol. 33, no. 7, pp. 1357–1380, 2015.

[11] L. Yao, Y.-W. A. Wu, L. Yao, and Z. Z. Liao, "An integrated imu and uwb sensor based indoor positioning system," in *2017 International Conference on Indoor Positioning and Indoor Navigation (IPIN)*. IEEE, 2017, pp. 1–8.

[12] Y. Zhong, T. Liu, B. Li, L. Yang, and L. Lou, "Integration of uwb and imu for precise and continuous indoor positioning," in *2018 Ubiquitous Positioning, Indoor Navigation and Location-Based Services (UPINLBS)*, 2018, pp. 1–5.

[13] C. Zhang, X. Bao, Q. Wei, Q. Ma, Y. Yang, and Q. Wang, "A kalman filter for uwb positioning in los/nlos scenarios," in *2016 Fourth International Conference on Ubiquitous Positioning, Indoor Navigation and Location Based Services (UPINLBS)*. IEEE, 2016, pp. 73–78.

[14] D. Feng, C. Wang, C. He, Y. Zhuang, and X.-G. Xia, "Kalman-filter-based integration of imu and uwb for high-accuracy indoor positioning and navigation," *IEEE Internet of Things Journal*, vol. 7, no. 4, pp. 3133–3146, 2020.

[15] Y. Wang and X. Li, "The imu/uwb fusion positioning algorithm based on a particle filter," *ISPRS International Journal of Geo-Information*, vol. 6, no. 8, p. 235, 2017.

[16] G. T. Lee, S. B. Seo, and W. S. Jeon, "Indoor localization by kalman filter based combining of uwb-positioning and pdr," in *2021 IEEE 18th Annual Consumer Communications & Networking Conference (CCNC)*. IEEE, 2021, pp. 1–6.

[17] N. Liu, R. Zhang, Z. Su, G. Fu, and J. He, "Research on wavelet threshold denoising method for uwb tunnel personnel motion location," *Mathematical Problems in Engineering*, vol. 2020, pp. 1–14, 2020.

[18] J. Li, T. Gao, X. Wang, D. Bai, and W. Guo, "The imu/uwb/odometer fusion positioning algorithm based on ekf," in *Journal of Physics: Conference Series*, vol. 2369, no. 1. IOP Publishing, 2022, p. 012092.

[19] Y. Liu, "Uwb ranging error analysis based on toa mode," in *Journal of Physics: Conference Series*, vol. 1939, no. 1. IOP Publishing, 2021, p. 012124.

[20] W. Guosheng, Q. Shuqi, L. Qiang, W. Heng, L. Huican, and L. Bing, "Uwb and imu system fusion for indoor navigation," in *2018 37th Chinese Control Conference (CCC)*. IEEE, 2018, pp. 4946–4950.

[21] X. Gui, S. Guo, Q. Chen, and L. Han, "A new calibration method of uwb antenna delay based on the ads-twr," in *2018 37th Chinese Control Conference (CCC)*, 2018, pp. 7364–7369.

[22] R. Fan and X. Du, "Nlos error mitigation using weighted least squares and kalman filter in uwb positioning," *arXiv preprint arXiv:2205.05939*, 2022.

[23] S. Wang, Y. Lyu, and W. Ren, "Unscented-transformation-based distributed nonlinear state estimation: Algorithm, analysis, and experiments," *IEEE Transactions on Control Systems Technology*, vol. 27, no. 5, pp. 2016–2029, 2019.

[24] M. Zhao, T. Zhang, and D. Wang, "A novel uwb positioning method based on a maximum-correntropy unscented kalman filter," *Applied Sciences*, vol. 12, no. 24, p. 12735, 2022.